







RESEARCH ARTICLE | DECEMBER 24 2024

Synchronization cluster bursting in adaptive oscillator networks

Special Collection: [Advances in Adaptive Dynamical Networks](#)

Mengke Wei ; Andreas Amann  ; Oleksandr Burylko ; Xiuqing Han; Serhiy Yanchuk ;
Jürgen Kurths 



Chaos 34, 123167 (2024)

<https://doi.org/10.1063/5.0226257>



Articles You May Be Interested In

How heterogeneity in connections and cycles matter for synchronization of complex networks

Chaos (November 2021)

Analysis of remote synchronization in complex networks

Chaos (October 2013)

Two-community noisy Kuramoto model with general interaction strengths. I

Chaos (March 2021)



Chaos

Special Topics Open for Submissions

[Learn More](#)

Synchronization cluster bursting in adaptive oscillator networks

Cite as: Chaos 34, 123167 (2024); doi: 10.1063/5.0226257

Submitted: 30 June 2024 · Accepted: 4 December 2024 ·

Published Online: 24 December 2024



View Online



Export Citation



CrossMark

Mengke Wei,^{1,2,3} Andreas Amann,^{2,4,a)} Oleksandr Burylko,^{2,5,6} Xiujiang Han,³ Serhiy Yanchuk,^{2,4} and Jürgen Kurths^{2,7}

AFFILIATIONS

¹School of Mathematical Science, Yangzhou University, Yangzhou 225002, China

²Potsdam Institute for Climate Impact Research, Telegrafenberg, Potsdam 14473, Germany

³Faculty of Civil Engineering and Mechanics, Jiangsu University, Zhenjiang 212013, China

⁴School of Mathematical Sciences, University College Cork, Cork T12 XF62, Ireland

⁵Institute of Mathematics, National Academy of Sciences of Ukraine, Kyiv 01024, Ukraine

⁶Institute of Mathematics, Humboldt University Berlin, Berlin 12489, Germany

⁷Research Institute of Intelligent Complex Systems, Fudan University, Shanghai 200433, China

Note: This paper is part of the Focus Issue on Advances in Adaptive Dynamical Networks.

a) Author to whom correspondence should be addressed: a.amann@ucc.ie

ABSTRACT

Adaptive dynamical networks are ubiquitous in real-world systems. This paper aims to explore the synchronization dynamics in networks of adaptive oscillators based on a paradigmatic system of adaptively coupled phase oscillators. Our numerical observations reveal the emergence of synchronization cluster bursting, characterized by periodic transitions between cluster synchronization and global synchronization. By investigating a reduced model, the mechanisms underlying synchronization cluster bursting are clarified. We show that a minimal model exhibiting this phenomenon can be reduced to a phase oscillator with complex-valued adaptation. Furthermore, the adaptivity of the system leads to the appearance of additional symmetries, and thus, to the coexistence of stable bursting solutions with very different Kuramoto order parameters.

Published under an exclusive license by AIP Publishing. <https://doi.org/10.1063/5.0226257>

Synchronization within dynamical systems of networks is frequently encountered in various fields of natural sciences and engineering technology. Recently, the study of synchronization of coupled systems has attracted extensive attention, and plenty of new patterns of network synchronization, such as complete synchronization, cluster synchronization, remote synchronization, and chimera states, have been reported. In particular, networks with adaptive couplings have emerged as a focal point of research due to their ability to model complex interactions more realistically. In this paper, we explore the synchronization dynamics of an adaptive oscillator network. Our results show that synchronization cluster bursting can be observed numerically in a paradigmatic system of adaptively coupled phase oscillators. We investigate the symmetries of the model and reduce the model to a normal form to reveal the mechanism of synchronization cluster bursting. Based on the dynamical analysis of the normal form

equation, we point out the role of fixed points in synchronization state transitions and the generation of bursting.

I. INTRODUCTION

The aspect of adaptivity^{1–5} has introduced a new dimension to the classic study of coupled oscillator networks. In an adaptive network, the coupling between oscillators evolves depending on the state of the system. The main motivation for studying adaptive networks stems from their importance in real world systems.^{4,6} For instance, in biological networks such as the human brain, synaptic plasticity allows for the strengthening or weakening of connections between neurons, facilitating learning and memory.^{7,8} Similarly, social networks exhibit adaptability, constantly reshaping connections to improve collective intelligence and accurate individual and

collective beliefs.⁹ Even in ecological networks, species adapt their behaviors in response to the changes in their habitat or population dynamics, thus promoting the stability of community dynamics.^{10,11} It is, therefore, important to understand the basic mechanisms of emergent collective behaviors and patterns in adaptive oscillator networks.^{12–14}

In many complex systems of coupled oscillators,^{15–20} it is possible to reduce much of the complexity by focusing on the dynamics of carefully chosen phase variables. The system is thus transformed into a model of coupled phase oscillators, which allows for a simplified analysis of the fundamental properties of the system. In this paper, we consider an adaptive version of the Kuramoto phase oscillator model. The classic Kuramoto model is an idealized model which has been successfully applied to coupled oscillator systems arising in physics,^{21–23} chemistry,^{24,25} electrical engineering,^{26–29} and other fields. The Kuramoto model and its many variations and extensions have been extensively studied in the literature. For example, an opinion changing rate model³⁰ was proposed by modifying the classical Kuramoto model to investigate the opinion synchronization in social networks. The Kuramoto model with phase lag was applied to the non-linear dynamics on a directed graph of a sequence of earthquakes.³¹ A number of recent reviews^{17,32–35} provide a detailed survey of the Kuramoto model, its extensions, and its most significant applications.

Synchronization,^{36–38} as a collective behavior among populations of dynamically interacting entities, has been extensively studied for its significant contributions in various fields, including biology,³⁹ ecology,⁴⁰ and sociology.⁴¹ It has been established that systems of coupled entities can exhibit various synchronization patterns.⁴² For example, recent studies of adaptive networks have revealed the phenomenon of recurrent synchronization,⁴³ a macroscopic event characterized by a periodic transition between synchronous and asynchronous behaviors. The underlying mechanisms of recurrent synchronization are attributed to the recurrent slow dynamics of hidden variables related to coupling weights, especially the asymmetry of adaptation rules. A more general chaotic recurrent clustering has been reported by Sales *et al.*⁴⁴ The concept of cluster synchronization,^{45–47} where the network is divided into synchronous sub-populations or clusters, is able to provide a framework for the understanding of dynamical coherence in coupled oscillatory systems. These clusters can dynamically form, dissolve, and even exhibit complex behaviors, such as synchronization cluster bursting, reflecting the rich interactions within the network. Bursting occurs when a system trajectory undergoes alternations between a rest state (silent phase) and an active state (repetitive spiking).^{48–50} In synchronization cluster bursting, different synchronization states appear and disappear in a burst-like manner, which has been frequently observed in various non-adaptive models.^{51–53} However, synchronization cluster bursting in adaptive networks has not yet been thoroughly investigated.

In this paper, we study the dynamics of an adaptive oscillator network based on an adaptive phase oscillator model. We conduct an analysis of the general model of N oscillators to reveal its key properties and symmetries. In particular, a new order parameter different from the standard Kuramoto order parameter is proposed which accounts for the symmetries of the model and allows us to better characterize synchronization. Then, we focus on the

numerical investigation of the model of three adaptive phase oscillators and demonstrate the distinct transitions between cluster synchronization and global synchronization. A useful quantity in this context is the time-dependent average frequency difference, which is used to identify the cluster synchronization state as a function of time. We discover that a quiescent state of the order parameter corresponds to global frequency synchronization, while oscillatory behavior indicates partial frequency synchronization. The transition between these two states gives rise to the effect of synchronization cluster bursting. Furthermore, we simplified the adaptive system into a reduced normal form equation. By conducting a systematic bifurcation and stability analysis of the normal form equation, we uncover the underlying mechanisms that give rise to synchronization cluster bursting.

II. MODEL OF ADAPTIVELY COUPLED OSCILLATORS

In this section, we will give a brief introduction to the adaptive phase oscillator model. First, we describe the general adaptive phase oscillator model with N oscillators in Subsec. II A. Then, we study symmetries of the general model in Subsec. II B. Finally, in Subsec. II C, we introduce an order parameter that respects the symmetries of the model.

A. General adaptive phase oscillator model

We begin this study by introducing a paradigmatic system of N coupled phase oscillators with adaptive coupling,^{18,54,55} which is given by

$$\begin{aligned}\dot{\varphi}_i &= \omega_i - \frac{1}{N} \sum_{j=1}^N \kappa_{ij} \sin(\varphi_i - \varphi_j), \\ \dot{\kappa}_{ij} &= -\varepsilon [\kappa_{ij} + A_{ij} \sin(\varphi_i - \varphi_j + \delta_{ij})].\end{aligned}\quad (1)$$

Here, $\varphi_i \in \mathbb{T}^1$ denotes the phase and ω_i is the natural frequency of oscillator i ($i = 1, \dots, N$). We use the notation \mathbb{T}^N for the N -dimensional torus. The interactions between the oscillators are quantified through the adaptive coupling weights, κ_{ij} , which represent the connection strength from the j th to the i th oscillator, where $i, j = 1, \dots, N$, $i \neq j$. The positive parameter ε is the rate of adaptation of the coupling weights. The parameters δ_{ij} are phase-lags of the adaptation function, and the coupling parameters $A_{ij} > 0$ represent an underlying topology. Therefore, we have an N^2 -dimensional phase space $(\varphi_1, \dots, \varphi_N, \kappa_{1,2}, \dots, \kappa_{1,N}, \dots, \kappa_{N,1}, \dots, \kappa_{N,N-1}) \in \mathbb{T}^N \times \mathbb{R}^{N(N-1)}$.

Note that, in this paper, we will choose the parameter ε to be small ($0 < \varepsilon \ll 1$), to obtain the case where the adaptation of the coupling weights is slow compared to the rapid dynamics of the phase oscillators, and thus, it is a slow-fast dynamical system.^{56–60} Moreover, the coupling weights remain confined within intervals $-A_{ij} \leq \kappa_{ij} \leq A_{ij}$ due to the existence of the attracting region $G = \{(\varphi_i, \kappa_{ij}) \in \mathbb{T}^N \times \mathbb{R}^{N(N-1)} : |\kappa_{ij}| \leq A_{ij}, i, j = 1, \dots, N\}$.¹⁸ In the following, we will study the model in the case of $A_{ij} \leq 1$, with ε fixed at 1.0×10^{-5} .

B. Symmetries of the general model

The model introduced in the previous section allows for the following non-trivial phase-space symmetries, which are crucial for the analysis of dynamics and synchronization.

1. Continuous phase shift symmetry

We note from the model equation (1) that only phase differences appear on the right side of the model equations. Therefore, the form of these equations will remain unchanged, if we add a constant phase shift to all oscillators. That is, the model has a continuous phase shift symmetry

$$\gamma_\sigma^c : \varphi_i \mapsto \varphi_i + \sigma, \quad (2)$$

for all $i = 1, \dots, N$ and $\sigma \in \mathbb{T}^1$.

2. Discrete phase space symmetry

From Eq. (1), we observe that a phase shift by π in the l th oscillator will change the signs of all sine terms that contain φ_l . This sign change is compensated, if we also change the signs of all those κ_{ij} with $i = l$ or $j = l$. More precisely, the system possesses the discrete phase space symmetries γ_l ($l = 1, \dots, N$), given by

$$\begin{aligned} \gamma_l^d : (\varphi_i; \kappa_{11}, \dots, \kappa_{Nl}, \kappa_{l1}, \dots, \kappa_{lN}) \\ \mapsto (\varphi_l + \pi; -\kappa_{1l}, \dots, -\kappa_{Nl}, -\kappa_{l1}, \dots, -\kappa_{lN}). \end{aligned} \quad (3)$$

Note that in (3), we only indicate the $2N - 1$ elements which are changed, and all other $(N - 1)^2$ variables remain unchanged. It is clear that $\gamma_l^d \circ \gamma_l^d = e$, where e is the identical operation, and $\gamma_l^d \circ \gamma_m^d = \gamma_m^d \circ \gamma_l^d$ for $l \neq m$. Therefore, the symmetry group generated by γ_l has 2^N elements and is isomorphic to $(\mathbb{Z}_2)^N = \mathbb{Z}_2 \times \dots \times \mathbb{Z}_2$. The continuous and discrete symmetries are connected through the relation $\gamma_\pi^c = \gamma_1^d \circ \gamma_2^d \circ \dots \circ \gamma_N^d$.

C. Order parameter

The standard Kuramoto order parameter $\tilde{R}(t)$ is given by⁶¹

$$\tilde{R}(t) = \frac{1}{N} \left| \sum_{j=1}^N e^{i\varphi_j(t)} \right|, \quad (4)$$

which is invariant under the symmetry operation γ_σ^c . However, it is not invariant under the discrete phase space symmetry operation γ_l^d since, in this case, one of the terms in Eq. (4) changes its sign. We, therefore, propose a different order parameter $R(t)$ that respects both discrete and continuous phase space symmetries, given by

$$R(t) = \frac{1}{N(N-1)} \left| \sum_{\substack{i,j=1 \\ i \neq j}}^N \kappa_{ij} e^{i(\varphi_i - \varphi_j)} \right|. \quad (5)$$

This order parameter obeys the two symmetry relations $R(t) \circ \gamma_\sigma^c = R(t)$ and $R(t) \circ \gamma_l^d = R(t)$ as desired and also fulfills the constraint

$$0 \leq R(t) \leq 1. \quad (6)$$

$R(t)$ can be interpreted as an averaged “synaptic input” of the system since it is an average of the real parts of the coupling terms in the phase dynamics from (1). It should be noted that $R(t)$ determines the degree of collective synchronization, while other aspects such as cluster synchronization can be represented by other measures, which will be introduced in Sec. IV A.

III. THREE ADAPTIVE PHASE OSCILLATORS

To investigate the synchronization cluster bursting in adaptive oscillator networks, we first focus on the case of three coupled phase oscillators. As shown in Fig. 1(a), the three oscillators φ_1 , φ_2 , and φ_3 are connected by the six adaptive coupling weights κ_{ij} ($i, j = 1, 2, 3$, $i \neq j$). The coupling parameters of the network are illustrated in Fig. 1(b).

A. System in phase difference variables

It is convenient to reduce the dimensionality of the model by introducing phase difference variables as illustrated in Fig. 1(c). We thus define

$$\theta_1 = \varphi_1 - \varphi_2, \quad \theta_2 = \varphi_1 - \varphi_3, \quad (7)$$

and the frequency differences

$$\Delta_1 = \omega_1 - \omega_2, \quad \Delta_2 = \omega_1 - \omega_3. \quad (8)$$

The original three phase oscillator model is transformed into the phase difference model,

$$\begin{aligned} \dot{\theta}_1 &= \Delta_1 - [(\kappa_{12} + \kappa_{21}) \sin \theta_1 + \kappa_{13} \sin \theta_2 + \kappa_{23} \sin(\theta_1 - \theta_2)]/3, \\ \dot{\theta}_2 &= \Delta_2 - [\kappa_{12} \sin \theta_1 + (\kappa_{13} + \kappa_{31}) \sin \theta_2 + \kappa_{32} \sin(\theta_2 - \theta_1)]/3, \\ \dot{\kappa}_{12} &= -\varepsilon[\kappa_{12} + A_{12} \sin(\theta_1 + \delta_{12})], \\ \dot{\kappa}_{13} &= -\varepsilon[\kappa_{13} + A_{13} \sin(\theta_2 + \delta_{13})], \\ \dot{\kappa}_{21} &= -\varepsilon[\kappa_{21} + A_{21} \sin(-\theta_1 + \delta_{21})], \\ \dot{\kappa}_{23} &= -\varepsilon[\kappa_{23} + A_{23} \sin(\theta_2 - \theta_1 + \delta_{23})], \\ \dot{\kappa}_{31} &= -\varepsilon[\kappa_{31} + A_{31} \sin(-\theta_2 + \delta_{31})], \\ \dot{\kappa}_{32} &= -\varepsilon[\kappa_{32} + A_{32} \sin(\theta_1 - \theta_2 + \delta_{32})]. \end{aligned} \quad (9)$$

B. Klein group symmetry K_4

While the symmetry operation γ_σ^c translates into the identity operation in the phase difference model, the original symmetries γ_l^d translate into non-trivial symmetries $\tilde{\gamma}_l^d$ as follows:

$$\begin{aligned} \tilde{\gamma}_1^d : (\theta_1, \theta_2, \kappa_{12}, \kappa_{13}, \kappa_{21}, \kappa_{23}, \kappa_{31}, \kappa_{32}) \\ \mapsto (\theta_1 + \pi, \theta_2 + \pi, -\kappa_{12}, -\kappa_{13}, -\kappa_{21}, \kappa_{23}, -\kappa_{31}, \kappa_{32}), \end{aligned} \quad (10)$$

$$\begin{aligned} \tilde{\gamma}_2^d : (\theta_1, \theta_2, \kappa_{12}, \kappa_{13}, \kappa_{21}, \kappa_{23}, \kappa_{31}, \kappa_{32}) \\ \mapsto (\theta_1 + \pi, \theta_2, -\kappa_{12}, \kappa_{13}, -\kappa_{21}, -\kappa_{23}, \kappa_{31}, -\kappa_{32}), \end{aligned} \quad (11)$$

$$\begin{aligned} \tilde{\gamma}_3^d : (\theta_1, \theta_2, \kappa_{12}, \kappa_{13}, \kappa_{21}, \kappa_{23}, \kappa_{31}, \kappa_{32}) \\ \mapsto (\theta_1, \theta_2 + \pi, \kappa_{12}, -\kappa_{13}, \kappa_{21}, -\kappa_{23}, -\kappa_{31}, -\kappa_{32}). \end{aligned} \quad (12)$$

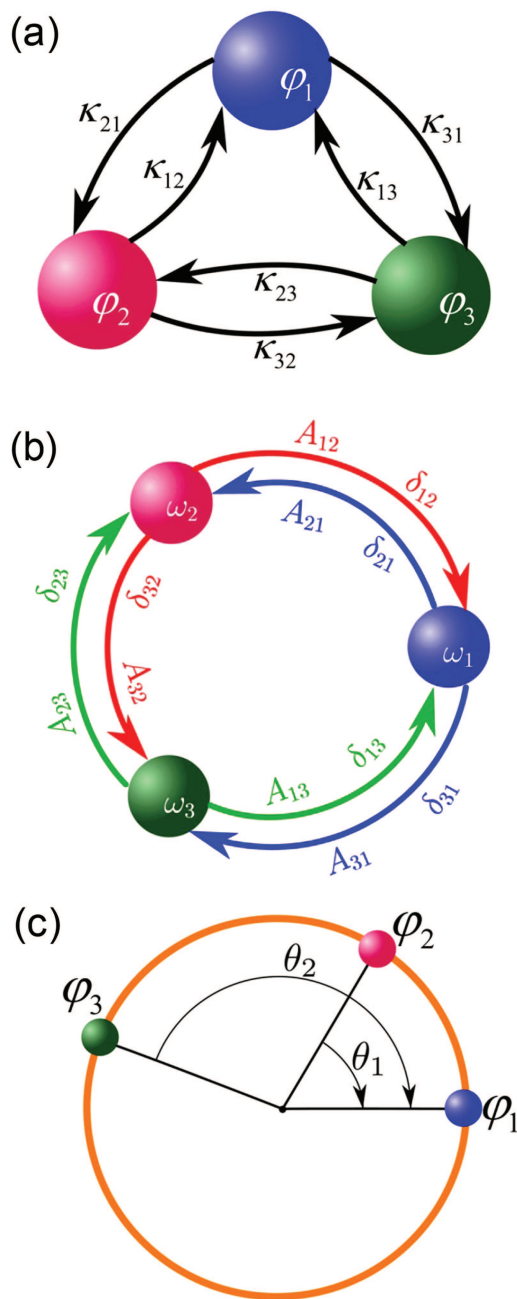


FIG. 1. (a) Schematic representation of the three coupled phase oscillators. (b) The oscillator network. (c) The phase differences.

These three actions together with the identity element e generate the Klein group of four elements:⁶² $\{e, \tilde{\gamma}_1^d, \tilde{\gamma}_2^d, \tilde{\gamma}_3^d\}$, which is commutative and has the properties $\tilde{\gamma}_i^d \circ \tilde{\gamma}_i^d = e$ and $\tilde{\gamma}_1^d \circ \tilde{\gamma}_2^d \circ \tilde{\gamma}_3^d = e$. The Klein-four group can be also represented as the direct product: $K_4 = \mathbb{Z}_2 \times \mathbb{Z}_2$.

IV. NUMERICAL OBSERVATION OF SYNCHRONIZATION CLUSTER BURSTING

In this section, we numerically demonstrate the existence of synchronization cluster bursting for the case of three adaptively coupled phase oscillators. We introduce the average frequency difference as a measure to determine the synchronization state among different oscillators of the system. Finally, we show how the symmetry of the system allows us to infer the existence of a second synchronization cluster state.

A. Synchronization cluster bursting

Here, we focus on the three oscillator adaptive phase model (9). In Figs. 2 and 3, we show a numerical scenario for the parameters given in Appendix A. We have numerically checked that the regime is robust in an open neighborhood of parameters. It is observed that the system exhibits periodic changes from fast repetitive spiking to an episode of steady dynamics, which can be regarded as bursting oscillations. At a given time t , the level of synchronization is measured by the order parameter $R(t)$. As shown in Fig. 2(a), the order parameter transitions between two distinct states: a nearly constant

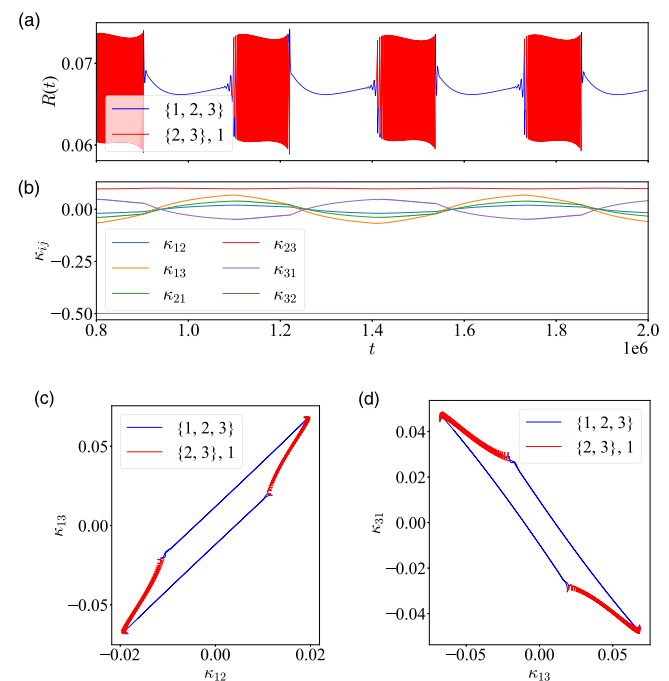


FIG. 2. Synchronization cluster bursting in the three adaptive phase oscillator model (9). Time series of order parameter R (a) and coupling weights κ_{ij} (b). Phase portraits in the coupling variables $(\kappa_{12}, \kappa_{13})$ (c) and $(\kappa_{13}, \kappa_{31})$ (d). The blue line, i.e., $\{1, 2, 3\}$, represents the three oscillators that are globally synchronized, while the red line, i.e., $\{2, 3\}, 1$, means that oscillators 2 and 3 are synchronized. All parameters are provided in Table I of Appendix A. The initial values of the variables were selected randomly. The particular values, which replicate this figure, are given in Table I.

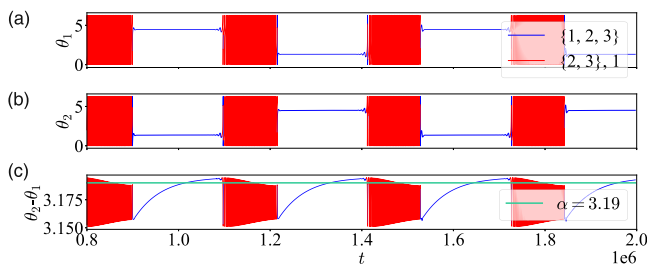


FIG. 3. Dynamics of the system in phase differences for three oscillators (9). Time series of θ_1 (a), θ_2 (b), and $\theta_2 - \theta_1$ (c).

value, representing the rest state of bursting, and a strongly oscillating order parameter indicating the active state of bursting. From Fig. 2(b), we see that the various coupling weights act quite differently during the transition between the oscillating and the rest state. While κ_{23} and κ_{32} remain approximately constant throughout, the other κ_{ij} engage in a low frequency oscillatory behavior around zero. When $R(t)$ oscillates, the coupling weights κ_{ij} also exhibit rapid fluctuations, but at a very small amplitude. In comparison, the oscillations of the phase differences $\theta_{1,2}$ presented in Fig. 3 are large during the oscillation phase of the order parameter. This indicates the presence of distinct timescales, with the coupling weights being the slow variables and the phase differences being the fast variables.

The observed changes of the order parameter over time in Fig. 2(a) as well as the evolution of the phase differences in Fig. 3 indicate transitions in the system's synchronization states. We would, therefore, characterize the time-dependent synchronization state of the system. Let us define the average frequency $\bar{\Omega}_i(t)$ of oscillator i at time t over some interval from $t - \Delta t/2$ to $t + \Delta t/2$ as

$$\bar{\Omega}_i(t) = \frac{\varphi_i(t - \frac{\Delta t}{2}) - \varphi_i(t + \frac{\Delta t}{2})}{\Delta t}, \quad (13)$$

where we choose a suitable Δt which is smaller than the timescale of the adaptive weights, but larger than the typical timescale of the phase variables. For our case, we choose $1 \leq \Delta t \leq \frac{1}{\epsilon}$. The frequency differences are then calculated as follows:

$$\bar{\Omega}_{ij}(t) = |\bar{\Omega}_i(t) - \bar{\Omega}_j(t)|. \quad (14)$$

We now stipulate that oscillators i and j are frequency synchronized at time t if the frequency difference is below some threshold parameter η , i.e., $\bar{\Omega}_{ij}(t) < \eta$. In this work, we chose $\eta = 1.0 \times 10^{-3}$. We then say that a set $\mathcal{C} = \{i_1, \dots, i_k\}$ forms a synchronization cluster, if each pair of oscillators in the set are frequency synchronized, i.e., if $\bar{\Omega}_{ij}(t) < \eta$ for all $i, j \in \mathcal{C}$. In the case of three oscillators, the notation $\{1, 2, 3\}$, therefore, indicates global frequency synchronization,⁴⁵ and the notation $\{i, j\}, k$ indicates partial frequency synchronization between oscillators i and j , but oscillator k not being part of the synchronization cluster.

Using the frequency difference $\bar{\Omega}_{ij}(t)$, we segment $R(t)$ into distinct sections, as shown in Fig. 2(a). Here, the blue line represents global frequency synchronization denoted by $\{1, 2, 3\}$, while the red line indicates partial frequency synchronization denoted by $\{2, 3\}, 1$. $R(t)$ periodically undergoes transitions between global

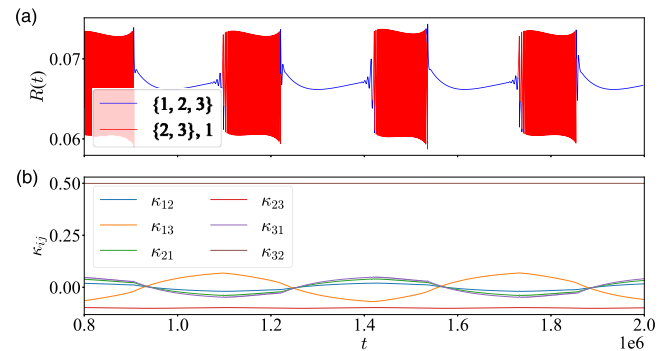


FIG. 4. The same as Fig. 2. Another synchronization cluster bursting pattern obtained through symmetry action $\tilde{\gamma}_2^d$. Time series of order parameter R (a) and coupling weights κ_{ij} (b).

synchronization and cluster synchronization in a burst-like manner. Such phenomena can be classified as synchronization cluster bursting. In particular, before global frequency synchronization terminates and partial frequency synchronization begins, $R(t)$ shows several distinct small oscillations. Moreover, it is observed from Figs. 3(a) and 3(b) that during global synchronization, the phase differences remain nearly constant. Conversely, in states of partial synchronization, the phase difference rotates between 0 and 2π . Similarly, small oscillations also occur when synchronization switches from global synchronization to partial synchronization. Finally, we like to point out that the phase difference between φ_2 and φ_3 is almost constant, i.e., $\theta_2 - \theta_1 \approx \pi$ [see Fig. 3(c)].

B. Alternative synchronization cluster bursting due to symmetry

The dynamics shown in Figs. 2 and 3 is not the only stable attractor of the system, and indeed, with different initial conditions, we find a second stable attractor as shown in Figs. 4 and 5. A comparison of the dynamics in either case reveals that applying the symmetry operation $\tilde{\gamma}_2^d$ provides a way to transition between the two attractors. This symmetry operation, in particular, flips the

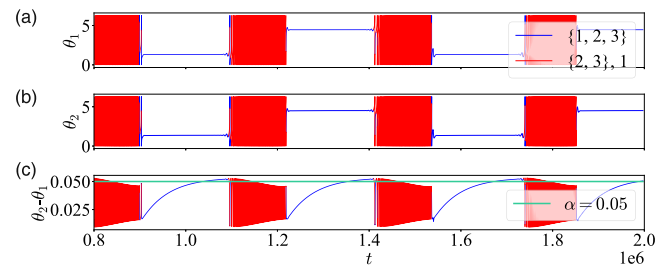


FIG. 5. The same as Fig. 3 for the case in Fig. 4, i.e., time series of θ_1 (a), θ_2 (b), and $\theta_2 - \theta_1$ (c).

signs of the almost constant κ_{23} and κ_{32} , and thereby create a manifestly different dynamical state. It also changes θ_1 by π and leaves θ_2 invariant, which explain why $\theta_2 - \theta_1 \approx 0$ in Fig. 5(c).

It is interesting to note that the symmetry operation $\tilde{\gamma}_1^d$, which changes both θ_1 and θ_2 by π , does not yield a new attractor when applied to the dynamics of Figs. 2 and 3. Instead, it induces a time shift by half a period on the same attractor. Similarly, because of $\tilde{\gamma}_2^d \circ \tilde{\gamma}_1^d = \tilde{\gamma}_3^d$, the application of $\tilde{\gamma}_3^d$ to the attractor in Figs. 2 and 3 yields a time-shifted version of the attractor in Figs. 4 and 5.

V. ANALYTICAL DESCRIPTION OF SYNCHRONIZATION CLUSTER BURSTING

In the following, we explain the mechanism of synchronization cluster bursting observed in the three oscillator adaptive phase model. By reducing the original model to an almost-invariant manifold, in Subsec. V A, we derive a simplified three-dimensional model, which is transformed into a normal form in Subsec. V B. The investigation of fixed points and bifurcations of the normal form equation enhance our understanding of the origin of the cluster bursting phenomena.

A. Reduction to an almost-invariant manifold

Based on the numerical observation, that in the cluster bursting attractors, the phase difference $\phi_2 - \phi_3 = \theta_2 - \theta_1$ is either close to π [see Fig. 3(c)] or close to 0 [Fig. 5(c)]. Let us use the approximation

$$\varphi_2(t) - \varphi_3(t) = \alpha, \quad (15)$$

where α is a positive parameter close to π or 0 (see Fig. 6). Based on this, we can simplify the original three oscillator model by replacing the phase variables φ_1, φ_2 , and φ_3 with φ_1 and $\frac{\varphi_2 + \varphi_3}{2}$. Then, by introducing the phase difference variable θ and the frequency difference parameter Δ via

$$\varphi_1 - \frac{\varphi_2 + \varphi_3}{2} = \theta, \quad w_1 - (w_2 + w_3)/2 = \Delta, \quad (16)$$

we obtain the reduced three-dimensional system

$$\begin{aligned} \dot{\theta} &= \Delta - \left[\kappa_1 \sin\left(\theta - \frac{\alpha}{2}\right) + \kappa_2 \sin\left(\theta + \frac{\alpha}{2}\right) + \beta \sin(\alpha) \right] / 3, \\ \dot{\kappa}_1 &= -\varepsilon \left[\kappa_1 + A_1 \sin\left(\theta - \frac{\alpha}{2} + \delta_1\right) \right], \\ \dot{\kappa}_2 &= -\varepsilon \left[\kappa_2 + A_2 \sin\left(\theta + \frac{\alpha}{2} + \delta_2\right) \right]. \end{aligned} \quad (17)$$

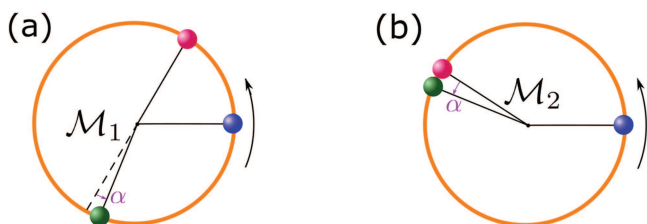


FIG. 6. Schematic representation of the phase difference between φ_2 and φ_3 . (a) α is close to π ; (b) α is close to 0.

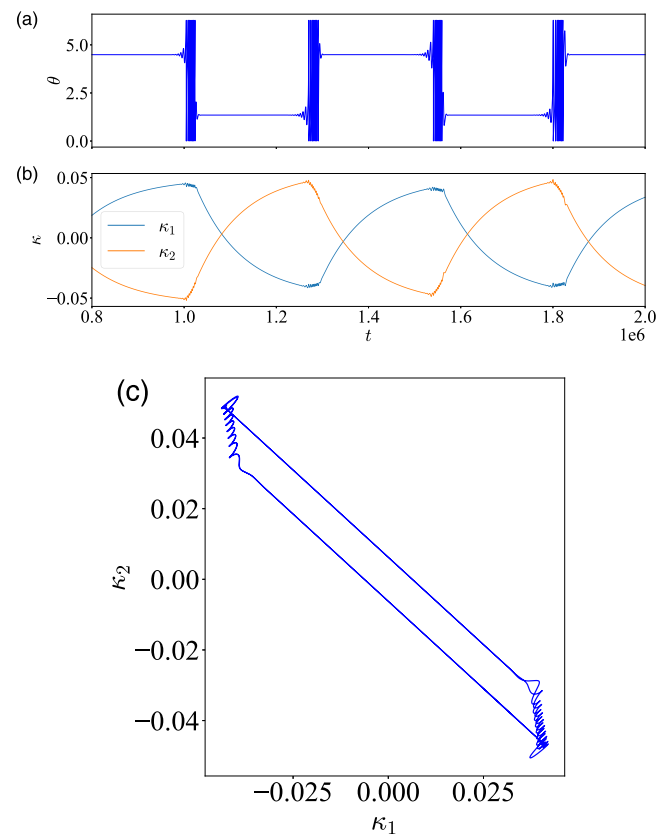


FIG. 7. Dynamics of the reduced three-dimensional system (17) for the case when α is fixed at 0.05 corresponding to the dynamics in Fig. 4. (a) Time series of θ . (b) Time series of coupling weights $\kappa_{1,2}$. (c) Phase portraits in the coupling variables (κ_1, κ_2) .

The expressions for the parameters $A_{1,2}$, $\delta_{1,2}$, and β in this reduced three-dimensional system (17) and their details can be found in Appendix B. As shown in the numerical result in Fig. 7, the dynamics of the reduced model retains the interesting bursting features of the original model, thus validating the effectiveness of the proposed reduction method.

B. Normal form equation

In order to facilitate the subsequent analysis of the underlying mechanisms of synchronization cluster bursting, we transform the model (17) to a normal form with a reduced number of parameters.

Note that

$$\kappa_1 \sin\left(\theta - \frac{\alpha}{2}\right) + \kappa_2 \sin\left(\theta + \frac{\alpha}{2}\right) = \text{Im} \left[\left[\kappa_1 e^{i(-\frac{\alpha}{2})} + \kappa_2 e^{i(+\frac{\alpha}{2})} \right] e^{i\theta} \right]. \quad (18)$$

The square bracket in the last equation is a complex number, parameterized by κ_1 and κ_2 . We can, therefore, replace the two equations for κ_1 and κ_2 in (17) with a single complex dynamical quantity. Then, by rescaling the equation, we transform system (17) into the normal

form

$$\begin{aligned}\dot{\theta} &= 1 - |Q| \sin(\theta - \phi_Q), \\ \dot{Q} &= -\hat{\varepsilon} [Q + C_1 e^{i\theta} + C_2 e^{-i\theta}],\end{aligned}\quad (19)$$

where $C_1, C_2 \in \mathbb{C}$, and $\hat{\varepsilon} \in \mathbb{R}$ are the parameters, $\theta \in \mathbb{T}^1$ and $Q \in \mathbb{C}$ are the dynamical variables, and ϕ_Q represents the argument of Q (see Appendix C for more details).

C. Dynamics of the normal form equation

With the above simplifications and reductions, we obtained a normal form for synchronization cluster bursting. The underlying mechanism of this effect is now revealed by analyzing the stability and bifurcation of the normal form equation (19) (see Appendix D for more details). First, we observe that the model allows for the following phase space and parameter symmetries:

$$(\theta, Q) \mapsto (\theta + \pi, -Q), \quad (20)$$

$$(\theta, Q, C_2) \mapsto (\theta + \sigma, Q e^{i\sigma}, C_2 e^{2i\sigma}), \quad (21)$$

where $\sigma \in \mathbb{T}^1$ is an arbitrary angle. As a result, we can change the phase of C_2 at the cost of adjusting the angle θ . We can use this symmetry to always choose $C_2 \in \mathbb{R}_0^+$. Thus, we have only four real parameters, i.e., $\hat{\varepsilon}$, $\text{Re}C_1$, $\text{Im}C_1$, and C_2 .

When the condition

$$|\text{Im}C_1 - 1| \leq C_2 \quad (22)$$

is satisfied [see also (D5) in Appendix D], there are, in general, four fixed points, with θ given by

$$\theta_{0,1} = \frac{\arcsin\left(\frac{\text{Im}C_1 - 1}{C_2}\right)}{2} \in \left(-\frac{\pi}{4}, \frac{\pi}{4}\right], \quad (23)$$

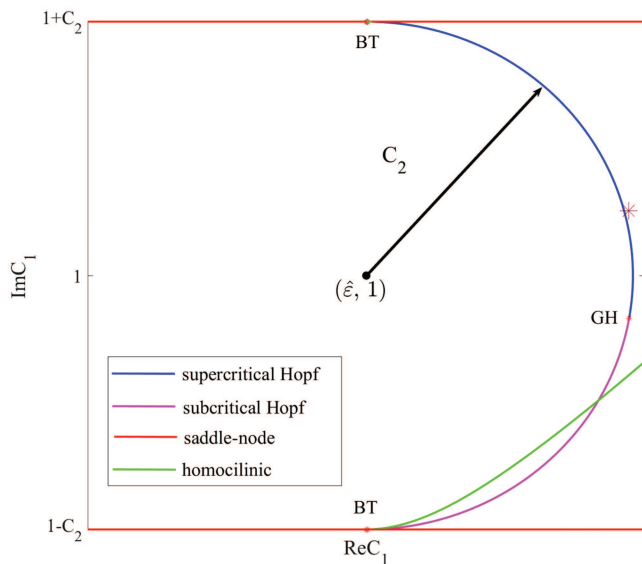


FIG. 8. Bifurcation set of the normal form equation (19) on the parameter plane ($\text{Re}C_1$, $\text{Im}C_1$). The asterisk marks the place where we study.

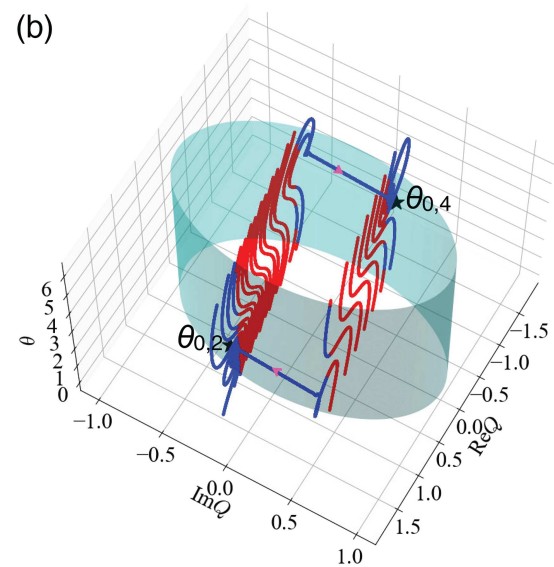
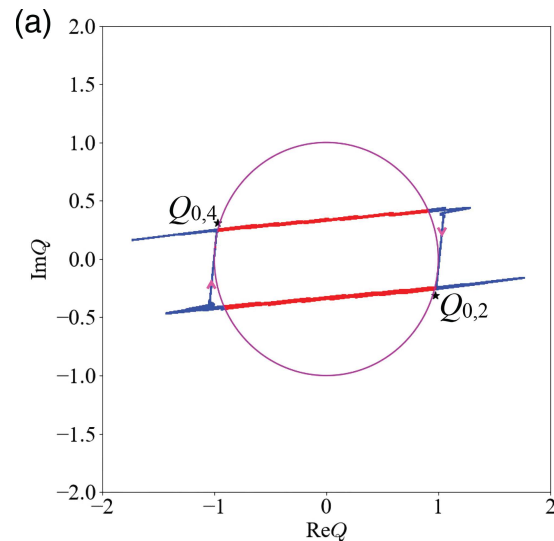


FIG. 9. Trajectory of the normal form equation (19) in the complex Q plane (a) and 3D space ($\text{Re}Q$, $\text{Im}Q$, θ) (b), where C_2 is assumed to be a positive real number by taking the modulus of the original complex number C_2 . The blue lines represent trajectories located outside the unit circle or cylinder, while red lines indicate trajectories within it. The pink arrows indicate the direction of motion of the trajectory, which is clockwise. The star markers represent unstable saddle-focus type fixed points.

$$\theta_{0,2} = \frac{\pi}{2} - \theta_{0,1} \in \left[\frac{\pi}{4}, 3\frac{\pi}{4}\right), \quad (24)$$

$$\theta_{0,3} = \theta_{0,1} + \pi \in \left(3\frac{\pi}{4}, 5\frac{\pi}{4}\right], \quad (25)$$

$$\theta_{0,4} = 3\frac{\pi}{2} - \theta_{0,1} \in \left[5\frac{\pi}{4}, 7\frac{\pi}{4}\right), \quad (26)$$

and the corresponding Q_0 given by

$$Q_{0,1} = -C_1 e^{i\theta_{0,1}} - C_2 e^{-i\theta_{0,1}}, \quad (27)$$

$$Q_{0,2} = -iC_1 e^{-i\theta_{0,1}} + iC_2 e^{i\theta_{0,1}}, \quad (28)$$

$$Q_{0,3} = -Q_{0,1}, \quad (29)$$

$$Q_{0,4} = -Q_{0,2}. \quad (30)$$

Based on this, we next present the results of the stability and bifurcation analyses of the fixed points, with a detailed analysis provided in [Appendix D](#). The result shows that $\theta_{0,1}$ and $\theta_{0,3}$ are saddle points with two unstable directions and one stable eigen-direction $\lambda_1 = -\hat{\varepsilon}$, while the stability of $\theta_{0,2}$ and $\theta_{0,4}$ depends on the sign of

$$T = \text{Re}C_1 + C_2 \cos 2\theta - \hat{\varepsilon}. \quad (31)$$

If $T < 0$, we have a stable node or focus with three stable directions; if $T > 0$, we have two unstable directions. The parameter point, where a saddle-node bifurcation occurs is given by

$$C_2 = |\text{Im}C_1 - 1|. \quad (32)$$

At $T = 0$, we have a Hopf bifurcation, which can be expressed as

$$|C_1 - (\hat{\varepsilon} + i)| = C_2. \quad (33)$$

This defines a circle in the complex C_1 plane with stable fixed points on the inside and only unstable fixed points on the outside, where the center of the circle is at $(\varepsilon, 1)$ and the radius is C_2 . Note that only one half of the circle corresponds to an actual Hopf bifurcation, while on the other half, the eigenvalues are real and have opposite signs.

Furthermore, we conducted a bifurcation analysis of the normal form equation (19) using MatCont software. As shown in [Fig. 8](#), we plot the bifurcation set on the parameter plan $(\text{Re}C_1, \text{Im}C_1)$, where the Hopf bifurcation curves and the homoclinic bifurcation curves terminate at a codimension 2 Bogdanov–Takens (BT) point on the saddle-node bifurcation curves. Additionally, the supercritical Hopf and subcritical Hopf bifurcations meet at the generalized Hopf (GH) point.

Note that the parameter combination we studied numerically in [Sec. IV](#) is located outside of the circle of Hopf bifurcation points (as shown in [Fig. 8](#) marked by the asterisk). Thus, the system only exhibits unstable fixed points including the two saddle-focus points $\theta_{0,2}$ and $\theta_{0,4}$. These unstable fixed points have one stable eigen-direction $\lambda_1 = -\hat{\varepsilon}$, and the (slowly) stable eigen-direction with

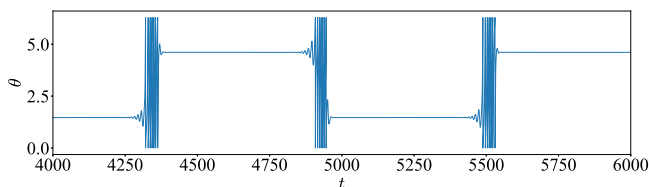


FIG. 10. Dynamics of θ in the normal form equation (19).

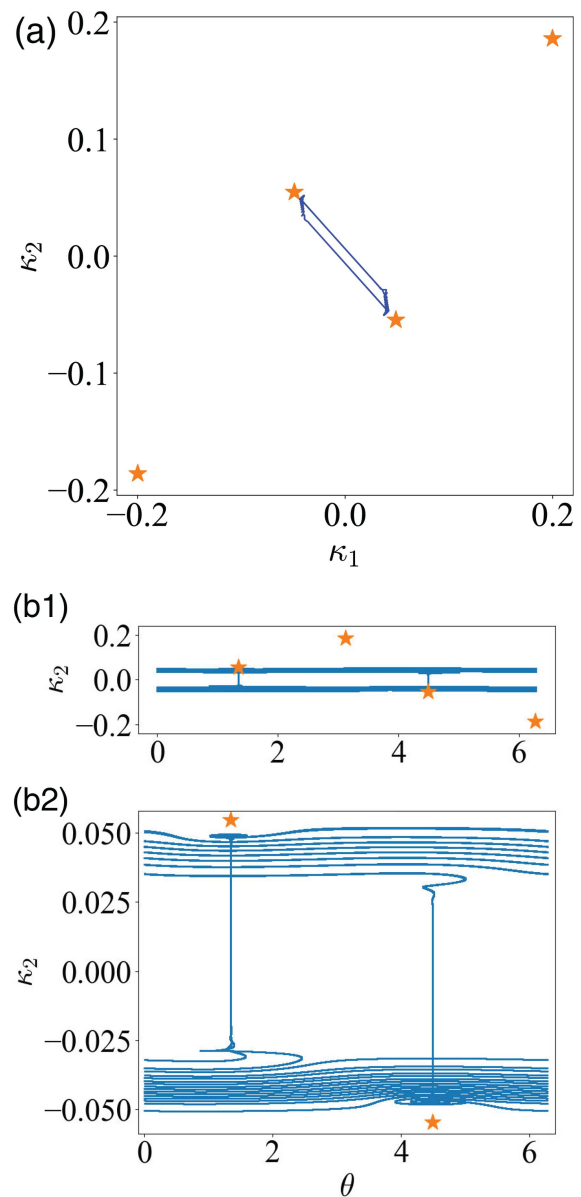


FIG. 11. The trajectory of the reduced three-dimensional model (17) in the $\kappa_1 - \kappa_2$ plane (a), and the $\theta - \kappa_2$ plane (b1) and its local enlargement (b2), in which the fixed points of the reduced three-dimensional model (17) is also superimposed.

which the trajectory approaches the fixed point is given by

$$v = \begin{pmatrix} 0 \\ \cos \theta \\ \sin \theta \end{pmatrix}. \quad (34)$$

Figure 9 gives an example when α is fixed at 0.05 corresponding to the synchronization cluster bursting in [Figs. 4](#) and [5](#) (when

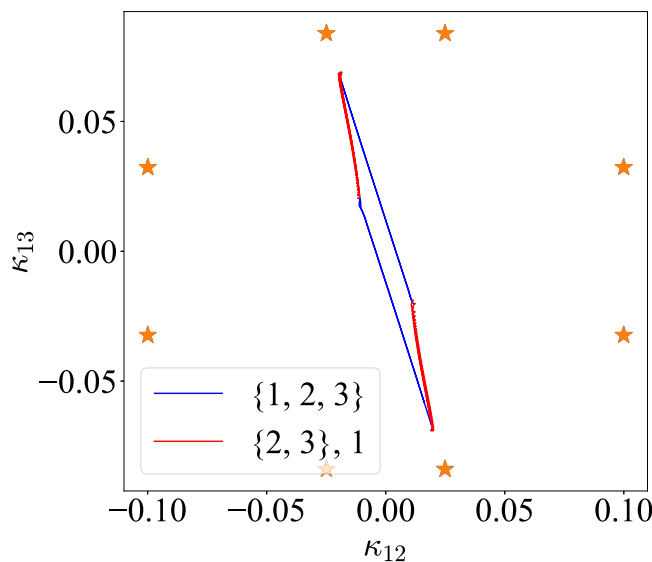


FIG. 12. The same as Fig. 4(c), in which the fixed points of the original three oscillator phase model are also superimposed.

$\alpha = 3.19$ corresponding to the synchronization cluster bursting in Figs. 2 and 3, the situation is also similar). In this case, the parameter values are fixed at $\text{Re}C_1 = 31.64$, $\text{Im}C_1 = 7.61$, $C_2 = 32.12$, and $\hat{\varepsilon} = 0.005$. It can be seen in Fig. 9(a) that, in the complex Q plane, outside the unit circle, the trajectory approaches the saddle-node fixed point along the eigen-direction (34), which is more clearly depicted in the three-dimensional representation shown in Fig. 9(b). This dynamical behavior corresponds to the near-horizontal segments in the time series θ (see Fig. 10). Because the situation we consider is close to the Hopf bifurcation, the trajectory spirals away from the saddle-focus and exhibits a libration, which explains the small-amplitude oscillations in the time series θ before large-amplitude oscillations take place as illustrated in Fig. 10. Then, it engages in a rotational motion ranging from 0 to 2π inside the cylinder, leading to large oscillations. Subsequently, it is attracted by another saddle-focus point. Based on this, we can explain the dynamics of θ as shown in Fig. 10, where small oscillatory motions without a full round trip (libration) and large oscillations ranging from 0 to 2π (rotation) can be observed. As a result, one can conclude that the saddle-focus fixed points $\theta_{0,2}$ and $\theta_{0,4}$ may play a crucial role in the generation of the synchronization cluster bursting in Fig. 4(a).

Note that the normal form (19) is derived from the reduced three-dimensional (17) through a linear transformation. Consequently, a similar phenomenon is evident in the (κ_1, κ_2) plane, where the trajectory also approaches unstable saddle-focus fixed points. Furthermore, this becomes more apparent in the enlarged view of the trajectory on the (θ, κ_2) plane, as depicted in Fig. 11.

Based on the analysis of the normal form equation, we have established that the fixed points, and in particular, the saddle points have a significant relevance for its dynamics. Next, the focus will shift to examining the fixed points of the original system (9) in

the κ -plane. By numerical fixed points analysis, we find eight fixed points (Fig. 12). These are categorized into two groups that can be derived from each other through Klein symmetry, with each group containing four points. Note that in the development of our three-dimensional model, the oscillators φ_2 and φ_3 are assumed to be coupled, which results in a loss of one symmetry, thereby reducing the count to four fixed points [see Fig. 11(a)]. In other words, saddle-node bifurcations occur among the fixed points across the two different groups when the model is reduced.

VI. CONCLUSION AND DISCUSSION

Cluster synchronization has been frequently reported in non-adaptive models. In this paper, we have investigated cluster synchronization even in the adaptive oscillator networks. As a result, synchronization cluster bursting has been revealed.

We first present a detailed analysis of the general adaptive phase oscillator model, and in particular, we identify the role of continuous phase shift symmetry and discrete phase space symmetry in the dynamics of the system. By introducing a different order parameter respecting both discrete and continuous phase space symmetries, we further quantify the synchronization level of the system.

We focused on the dynamics of the three adaptive phase oscillators and uncovered the influence of the Klein group symmetry K_4 on the system's behavior. Our numerical observations have demonstrated the emergence of synchronization cluster bursting, offering new insights into the mechanisms of synchronization in complex networks. The time-dependent average frequency difference helps us to understand the synchronization cluster bursting and allows us to observe the system transitions between global and cluster synchronization. Then, we derive alternative synchronization cluster bursting from the Klein group symmetry K_4 , which deepens our understanding of synchronization cluster bursting in adaptive oscillator networks.

The reduction to the almost-invariant manifold and the derivation of the normal form equation for the three adaptive phase oscillators provided a more streamlined analytical framework for this complex dynamics. Moreover, we have engaged in a detailed discussion of the dynamics of the normal form to reveal the underlying mechanism of synchronization cluster bursting. The results show that the saddle-focus fixed points play a key role in the emergence of synchronization cluster bursting, near which the system's trajectory undergoes dramatic changes. It first directly approaches the saddle-node fixed point along the eigen-direction. Then, the trajectory spirals away from the saddle-focus creating libration, and finally, evolving into rotation. Subsequently, the trajectory is drawn to another saddle-focus point. Therefore, the presence of saddle-focus fixed points introduces a mechanism by which the system can transition from a state of global synchronization to that of partial synchronization and back.

While, in this paper, we focus on the case of small but finite ε , it is also interesting to consider the limiting case of $\varepsilon \rightarrow 0$. In this case, the theory of slow-fast systems^{56–60} can be employed, and in⁴³, it was found that the dynamics of two adaptively coupled oscillators can be reduced to a non-smooth system in the (κ_1, κ_2) plane after eliminating the fast θ variable. The critical manifold in the case of two

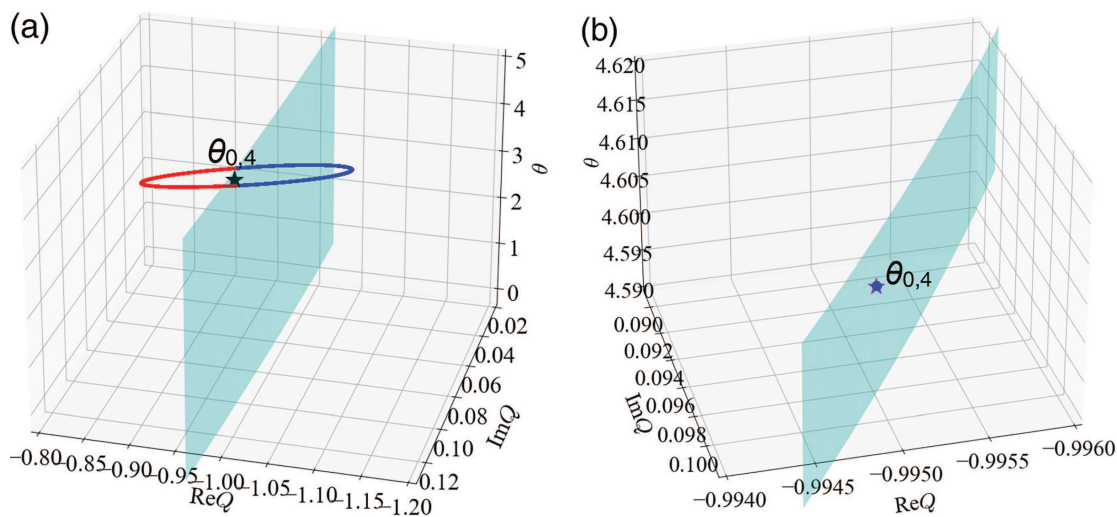


FIG. 13. Evolution of the trajectory with the decrease of $\text{Re}C_1$ near the point marked by the asterisk in Fig. 8. (a) $\text{Re}C_1 = 31.44$, $\theta_{0,4}$ is unstable and there exists a stable limit cycle attractor originated from the supercritical Hopf bifurcation. (b) $\text{Re}C_1 = 31.43$, $\theta_{0,4}$ is a stable fixed point.

oscillators corresponds to either a stable fixed point or an oscillating solution in θ . In the case of three adaptively coupled oscillators, the critical manifold can be more complex and can include fixed points, and limit cycle solutions on the (θ_1, θ_2) torus. This is outside of the scope of the current paper.

Besides, we would like to point out that the variations in parameters induce alterations in the trajectory near the point indicated by the asterisk in Fig. 8. For example, it can be seen in Fig. 13 that, if the parameters we consider are extremely close to the Hopf bifurcation, a stable limit cycle attractor that originated from the supercritical Hopf bifurcation can be created and the trajectory is attracted by the stable limit cycle exhibiting libration. While if the parameter is inside the semicircle formed by the Hopf bifurcation curve in Fig. 8, two stable fixed points $\theta_{0,2}$ and $\theta_{0,4}$ occur and the trajectory will be attracted by one of them without libration and rotation.

Finally, it is clear that there are many issues that deserve in-depth exploration in future. For instance, how to extend our model to larger-scale networks and how to analyze the mechanism of synchronization cluster bursting therein are key questions for future works. In this manuscript, we have studied synchronization cluster bursting in three adaptively coupled systems. This regime is robust as it occurs for an open set of parameters. Other regimes have also been reported in Ref. 44. An interesting open question is whether it is possible to obtain an exhaustive list of regimes in such a system, but this question is beyond the scope of this work.

ACKNOWLEDGMENTS

This work was supported by the Deutsche Forschungsgemeinschaft (DFG, German Research Foundation), Project No. 411803875. M.W. acknowledges support from the China Scholarship Council (CSC) scholarship (Grant No. 202208320297). A.A. acknowledges support from PIK Werkvertrag 2023-0336. O.B. acknowledges hospitality at PIK and HU, as well as support through

the DFG via project 195170736—SFB/TRR 109. X.H. acknowledges support from the National Natural Science Foundation of China (Grant Nos. 12272150 and 12072132). The authors would like to thank Matheus Rolim Sales for discussions and numerical studies during the initial phase of the project. The authors express their gratitude to the anonymous reviewers whose comments and suggestions have helped to improve this paper.

AUTHOR DECLARATIONS

Conflict of Interest

The authors have no conflicts to disclose.

Author Contributions

Mengke Wei: Conceptualization (equal); Methodology (equal); Writing – original draft (equal). **Andreas Amann:** Methodology (equal); Supervision (equal); Writing – review & editing (equal). **Oleksandr Burylko:** Methodology (equal); Writing – review & editing (equal). **Xiujing Han:** Supervision (equal). **Serhiy Yanchuk:** Methodology (equal); Supervision (equal); Writing – review & editing (equal). **Jürgen Kurths:** Methodology (equal); Supervision (equal); Writing – review & editing (equal).

DATA AVAILABILITY

The data that support the findings of this study are available from the corresponding author upon reasonable request.

APPENDIX A: INITIAL VALUES AND PARAMETER VALUES CORRESPONDING TO FIG. 2

To replicate the numerical simulation presented in Fig. 2, the initial values and parameter settings used are outlined in Table I.

TABLE I. Initial values and parameter values.

Initial values		
$\varphi_1 = 6.281\,21$	$\kappa_{12} = 0.413\,73$	$\kappa_{23} = -0.151\,08$
$\varphi_2 = 3.744\,88$	$\kappa_{13} = -0.333\,69$	$\kappa_{31} = 0.081\,16$
$\varphi_3 = 3.401\,65$	$\kappa_{21} = 0.273\,33$	$\kappa_{32} = 0.023\,94$
Parameter values		
$\delta_{12} = 0.5\pi$	$A_{12} = 0.1$	$\omega_1 = 0.012$
$\delta_{13} = 0.88\pi$	$A_{13} = 0.1$	$\omega_2 = 0.007$
$\delta_{21} = 0.5\pi$	$A_{21} = 0.2$	$\omega_3 = 0.003$
$\delta_{23} = 0.88\pi$	$A_{23} = 0.3$	$\varepsilon = 1.0 \times 10^{-5}$
$\delta_{31} = 0.5\pi$	$A_{31} = 0.3$	
$\delta_{32} = 1.5\pi$	$A_{32} = 0.5$	

APPENDIX B: EXPRESSIONS FOR PARAMETERS IN THE REDUCED SYSTEM

Based on the phase difference and frequency difference in (16), it holds that

$$\begin{aligned}
 \dot{\theta} &= \Delta - \frac{1}{3} \left[\left(\kappa_{12} + \frac{\kappa_{21}}{2} \right) \sin \left(\theta - \frac{\alpha}{2} \right) + \left(\kappa_{13} + \frac{\kappa_{31}}{2} \right) \sin \left(\theta + \frac{\alpha}{2} \right) + \left(\frac{\kappa_{32}}{2} - \frac{\kappa_{23}}{2} \right) \sin(\alpha) \right], \\
 \dot{\kappa}_{12} &= -\varepsilon \left[\kappa_{12} + A_{12} \sin \left(\theta - \frac{\alpha}{2} + \delta_{12} \right) \right], \\
 \dot{\kappa}_{13} &= -\varepsilon \left[\kappa_{13} + A_{13} \sin \left(\theta + \frac{\alpha}{2} + \delta_{13} \right) \right], \\
 \dot{\kappa}_{21} &= -\varepsilon \left[\kappa_{21} - A_{21} \sin \left(\theta - \frac{\alpha}{2} - \delta_{21} \right) \right], \\
 \dot{\kappa}_{23} &= -\varepsilon \left[\kappa_{23} + A_{23} \sin(\alpha + \delta_{23}) \right], \\
 \dot{\kappa}_{31} &= -\varepsilon \left[\kappa_{31} - A_{31} \sin \left(\theta + \frac{\alpha}{2} - \delta_{31} \right) \right], \\
 \dot{\kappa}_{32} &= -\varepsilon \left[\kappa_{32} - A_{32} \sin(\alpha - \delta_{32}) \right].
 \end{aligned} \quad (B1)$$

By letting

$$\kappa_1 = \kappa_{12} + \frac{\kappa_{21}}{2}, \quad \kappa_2 = \kappa_{13} + \frac{\kappa_{31}}{2}, \quad \kappa_3 = -\frac{\kappa_{23}}{2} + \frac{\kappa_{32}}{2}, \quad (B2)$$

to combine κ_{ij} and κ_{ji} , the above equation can be further simplified as

$$\begin{aligned}
 \dot{\theta} &= \Delta - \left[\kappa_1 \sin \left(\theta - \frac{\alpha}{2} \right) + \kappa_2 \sin \left(\theta + \frac{\alpha}{2} \right) + \kappa_3 \sin(\alpha) \right] / 3, \\
 \dot{\kappa}_1 &= -\varepsilon \left[\kappa_1 + A_{12} \sin \left(\theta - \frac{\alpha}{2} + \delta_{12} \right) - \frac{A_{21}}{2} \sin \left(\theta - \frac{\alpha}{2} - \delta_{21} \right) \right], \\
 \dot{\kappa}_2 &= -\varepsilon \left[\kappa_2 + A_{13} \sin \left(\theta + \frac{\alpha}{2} + \delta_{13} \right) - \frac{A_{31}}{2} \sin \left(\theta + \frac{\alpha}{2} - \delta_{31} \right) \right], \\
 \dot{\kappa}_3 &= -\varepsilon \left[\kappa_3 - \frac{A_{23}}{2} \sin(\alpha + \delta_{23}) - \frac{A_{32}}{2} \sin(\alpha - \delta_{32}) \right].
 \end{aligned} \quad (B3)$$

Since κ_3 is a constant, i.e.,

$$\kappa_3 = \frac{A_{23}}{2} \sin(\alpha + \delta_{23}) + \frac{A_{32}}{2} \sin(\alpha - \delta_{32}), \quad (B4)$$

we can obtain the simplified three-dimensional system

$$\begin{aligned}
 \dot{\theta} &= \Delta - \frac{1}{3} \left[\kappa_1 \sin \left(\theta - \frac{\alpha}{2} \right) + \kappa_2 \sin \left(\theta + \frac{\alpha}{2} \right) + \left(\frac{A_{23}}{2} \sin(\alpha + \delta_{23}) + \frac{A_{32}}{2} \sin(\alpha - \delta_{32}) \right) \sin(\alpha) \right], \\
 \dot{\kappa}_1 &= -\varepsilon \left[\kappa_1 + A_{12} \sin \left(\theta - \frac{\alpha}{2} + \delta_{12} \right) - \frac{A_{21}}{2} \sin \left(\theta - \frac{\alpha}{2} - \delta_{21} \right) \right], \\
 \dot{\kappa}_2 &= -\varepsilon \left[\kappa_2 + A_{13} \sin \left(\theta + \frac{\alpha}{2} + \delta_{13} \right) - \frac{A_{31}}{2} \sin \left(\theta + \frac{\alpha}{2} - \delta_{31} \right) \right],
 \end{aligned} \quad (B5)$$

which can further be reformulated into the form of Eq. (17), where

$$\beta = [A_{23} \sin(\alpha + \delta_{23}) + A_{32} \sin(\alpha - \delta_{32})] / 2, \quad (B6)$$

$$A_1 = \sqrt{(A_{12} \cos(\delta_{12}) - 0.5A_{21} \cos(\delta_{21}))^2 + (A_{12} \sin(\delta_{12}) + 0.5A_{21} \sin(\delta_{21}))^2}, \quad (B7)$$

$$\delta_1 = \arctan \left(\frac{A_{12} \sin(\delta_{12}) + 0.5A_{21} \sin(\delta_{21})}{A_{12} \cos(\delta_{12}) - 0.5A_{21} \cos(\delta_{21})} \right), \quad (B8)$$

$$A_2 = \sqrt{(A_{13} \cos(\delta_{13}) - 0.5A_{31} \cos(\delta_{31}))^2 + (A_{13} \sin(\delta_{13}) + 0.5A_{31} \sin(\delta_{31}))^2}, \quad (B9)$$

$$\delta_2 = \arctan \left(\frac{A_{13} \sin(\delta_{13}) + 0.5A_{31} \sin(\delta_{31})}{A_{13} \cos(\delta_{13}) - 0.5A_{31} \cos(\delta_{31})} \right). \quad (B10)$$

APPENDIX C: DERIVATION OF NORMAL FORM EQUATION

We can replace the two kappas in system (17) with a single complex dynamical quantity

$$\check{Q}^* = \kappa_1 e^{i(-\frac{\alpha}{2})} + \kappa_2 e^{i(\frac{\alpha}{2})}. \quad (C1)$$

This means that the equation for θ becomes

$$\dot{\theta} = \Delta - [\text{Im} \{ \check{Q}^* e^{i\theta} \} + \beta \sin(\alpha)]/3. \quad (C2)$$

Then, the derive equation for \check{Q} (\check{Q}^* is the complex conjugate of \check{Q}) can be given by

$$\dot{\check{Q}} = \kappa_1 e^{i(\frac{\alpha}{2})} + \kappa_2 e^{i(-\frac{\alpha}{2})} \quad (C3)$$

$$= e^{i(\frac{\alpha}{2})} \left\{ -\varepsilon \left[\kappa_1 + A_1 \sin \left(\theta - \frac{\alpha}{2} + \delta_1 \right) \right] \right. \\ \left. + e^{i(-\frac{\alpha}{2})} \left\{ -\varepsilon \left[\kappa_2 + A_2 \sin \left(\theta + \frac{\alpha}{2} + \delta_2 \right) \right] \right\} \right\} \quad (C4)$$

$$= -\varepsilon \left[\kappa_1 e^{i(\frac{\alpha}{2})} + A_1 e^{i(\frac{\alpha}{2})} \sin \left(\theta - \frac{\alpha}{2} + \delta_1 \right) \right. \\ \left. + \kappa_2 e^{i(-\frac{\alpha}{2})} + A_2 e^{i(-\frac{\alpha}{2})} \sin \left(\theta + \frac{\alpha}{2} + \delta_2 \right) \right] \quad (C5)$$

$$= -\varepsilon \left[\check{Q} + A_1 e^{i(\frac{\alpha}{2})} \sin \left(\theta - \frac{\alpha}{2} + \delta_1 \right) \right. \\ \left. + A_2 e^{i(-\frac{\alpha}{2})} \sin \left(\theta + \frac{\alpha}{2} + \delta_2 \right) \right]. \quad (C6)$$

Based on

$$e^{ix} = \cos(x) + i \sin(x), \quad (C7)$$

we can get

$$\sin(x) = \frac{e^{ix} - e^{-ix}}{2i}. \quad (C8)$$

For the first term

$$A_1 e^{i(\frac{\alpha}{2})} \sin \left(\theta - \frac{\alpha}{2} + \delta_1 \right), \quad (C9)$$

we can expand it as

$$\frac{A_1}{2i} \left[e^{i(\theta+\delta_1)} - e^{-i(\theta+\delta_1-\alpha)} \right]. \quad (C10)$$

For the second term

$$A_2 e^{i(-\frac{\alpha}{2})} \sin \left(\theta + \frac{\alpha}{2} + \delta_2 \right), \quad (C11)$$

we can expand it as

$$\frac{A_2}{2i} \left[e^{i(\theta+\delta_2)} - e^{-i(\theta+\delta_2+\alpha)} \right]. \quad (C12)$$

Combining the two terms and extracting coefficients associated with $e^{i\theta}$ and $e^{-i\theta}$, we obtain

$$A_1 e^{i(\frac{\alpha}{2})} \sin \left(\theta - \frac{\alpha}{2} + \delta_1 \right) + A_2 e^{i(-\frac{\alpha}{2})} \sin \left(\theta + \frac{\alpha}{2} + \delta_2 \right) \\ = \check{C}_1 e^{i\theta} + \check{C}_2 e^{-i\theta}. \quad (C13)$$

As a result, the derive equation for \check{Q} is

$$\dot{\check{Q}} = -\varepsilon \left[\check{Q} + \check{C}_1 e^{i\theta} + \check{C}_2 e^{-i\theta} \right], \quad (C14)$$

where

$$\check{C}_1 = \frac{1}{2i} (A_1 e^{i\delta_1} + A_2 e^{i\delta_2}) = (A_1 \sin \delta_1 + A_2 \sin \delta_2) / 2 \\ - i (A_1 \cos \delta_1 + A_2 \cos \delta_2) / 2, \quad (C15)$$

$$\check{C}_2 = -\frac{1}{2i} [A_1 e^{-i(\delta_1-\alpha)} + A_2 e^{-i(\delta_2+\alpha)}] \\ = [A_1 \sin(\delta_1 - \alpha) + A_2 \sin(\delta_2 + \alpha)] / 2 \\ + i [A_1 \cos(\delta_1 - \alpha) + A_2 \cos(\delta_2 + \alpha)] / 2,$$

are complex constants. Furthermore, if we absorb the β term into $|\Delta|$, we can define

$$\check{\Delta} = \Delta - \frac{1}{3} \beta \sin(\alpha). \quad (C16)$$

Let us define a new timescale τ such that

$$d\tau = \left| \check{\Delta} \right| dt. \quad (C17)$$

Then, setting $\hat{\varepsilon} = \frac{\varepsilon}{\check{\Delta}}$, $C_1 = \frac{\check{C}_1}{3\check{\Delta}}$, $C_2 = \frac{\check{C}_2}{3\check{\Delta}}$, the rescaled equation in terms of τ becomes

$$\dot{\theta} = 1 - |Q| \sin(\theta - \phi_Q), \quad (C18)$$

$$\dot{Q} = -\hat{\varepsilon} [Q + C_1 e^{i\theta} + C_2 e^{-i\theta}],$$

where $C_1, C_2 \in \mathbb{C}$, and $\hat{\varepsilon} \in \mathbb{R}$ are parameters, $\theta \in \mathbb{S}^1$ and $Q \in \mathbb{C}$ are the dynamical variables, and ϕ_Q represents the argument of Q .

APPENDIX D: DERIVATION OF FIXED POINTS OF THE NORMAL FORM EQUATION AND THEIR STABILITY ANALYSIS

1. Fixed points

Let us study the fixed points of the normal form (19) in detail. If (θ_0, Q_0) is a fixed point of (19), then

$$1 = \text{Im} Q_0^* e^{i\theta_0}, \quad (D1)$$

$$-Q_0 = C_1 e^{i\theta_0} + C_2 e^{-i\theta_0}. \quad (D2)$$

Plugging the second equation into the first gives

$$1 = -\text{Im} [(C_1 e^{i\theta_0} + C_2 e^{-i\theta_0})^* e^{i\theta_0}] \\ = -\text{Im} [C_1^* + C_2 e^{i2\theta_0}] \\ = \text{Im} C_1 - C_2 \sin 2\theta_0. \quad (D3)$$

This yields the condition

$$\sin 2\theta_0 = \frac{\text{Im} C_1 - 1}{C_2}, \quad (D4)$$

which can only be fulfilled if

$$|\text{Im} C_1 - 1| \leq C_2. \quad (D5)$$

As a result, we can obtain four fixed points: (23)–(30).

2. Saddle-node bifurcation

We can plot the area in which (D5) is fulfilled in a graph with $\text{Im}C_1$ on the x axis and C_2 on the y axis. This is an area above the line

$$C_2 = |\text{Im}C_1 - 1|. \quad (\text{D6})$$

This line has two parts: one with slope 1 for $\text{Im}C_1 > 1$, and one with slope -1 else. As we approach this line from above, the four fixed points merge in pairs and vanish as we cross the line. Thus, this line denotes a saddle-node bifurcation. More precisely, we have for $\text{Im}C_1 > 1$

$$\theta_{0,1} \nearrow \frac{\pi}{4}, \quad (\text{D7})$$

$$\theta_{0,2} \searrow \frac{\pi}{4}, \quad (\text{D8})$$

$$\theta_{0,3} \nearrow 5\frac{\pi}{4}, \quad (\text{D9})$$

$$\theta_{0,4} \searrow 5\frac{\pi}{4}. \quad (\text{D10})$$

At the point where this saddle-node bifurcation happens, we have

$$\begin{aligned} Q_{0,1} &= -C_1 e^{i\theta_{0,1}} - C_2 e^{-i\theta_{0,1}} \\ &= -C_1 e^{i\frac{\pi}{4}} - (\text{Im}C_1 - 1) e^{-i\frac{\pi}{4}} \\ &= \frac{-C_1 (1+i) - (\text{Im}C_1 - 1)(1-i)}{\sqrt{2}} \\ &= \frac{-(\text{Re}C_1 + i\text{Im}C_1)(1+i) - (\text{Im}C_1 - 1)(1-i)}{\sqrt{2}} \\ &= \frac{-(\text{Re}C_1)(1+i) + (1-i)}{\sqrt{2}} \\ &= \frac{1 - \text{Re}C_1 - i(1 + \text{Re}C_1)}{\sqrt{2}}, \\ Q_{0,2} &= -iC_1 e^{-i\theta_{0,1}} + iC_2 e^{i\theta_{0,1}}, \\ &= -iC_1 e^{-i\frac{\pi}{4}} + i[\text{Im}C_1 - 1] e^{i\frac{\pi}{4}} = Q_{0,1}, \end{aligned} \quad (\text{D11})$$

$$Q_{0,3} = -Q_{0,1}$$

$$Q_{0,4} = -Q_{0,2} = Q_{0,1}.$$

Also note that

$$|Q_{0,1}|^2 = 1 + (\text{Re}C_1)^2 \quad (\text{D12})$$

and similar for all other fixed points. This means that the saddle-node bifurcation happens outside of the unit circle. It is, therefore, different from the naïve saddle-node bifurcation in the θ dynamics, which happens at $|Q| = 1$.

3. Stability of fixed points

In order to assess the stability of the fixed points, we need to consider the Jacobian matrix of our system. To do this, let us introduce $\text{Re}Q$ and $\text{Im}Q$,

$$Q = \text{Re}Q + i\text{Im}Q, \quad (\text{D13})$$

$$|Q| = \sqrt{\text{Re}Q^2 + \text{Im}Q^2}, \quad (\text{D14})$$

$$\phi_Q = \arctan \frac{\text{Im}Q}{\text{Re}Q}. \quad (\text{D15})$$

This gives the three-dimensional real system

$$\dot{\theta} = 1 - (\text{Re}Q \sin \theta - \text{Im}Q \cos \theta), \quad (\text{D16})$$

$$\text{Re}\dot{Q} = -\hat{\varepsilon} [\text{Re}Q + (\text{Re}C_1 + C_2) \cos \theta - \text{Im}C_1 \sin \theta], \quad (\text{D17})$$

$$\text{Im}\dot{Q} = -\hat{\varepsilon} [\text{Im}Q + \text{Im}C_1 \cos \theta + (\text{Re}C_1 - C_2) \sin \theta]. \quad (\text{D18})$$

We get the Jacobian matrix

$$J = \begin{pmatrix} -(\text{Re}Q \cos \theta + \text{Im}Q \sin \theta) & -\sin \theta & \cos \theta \\ \hat{\varepsilon} [(\text{Re}C_1 + C_2) \sin \theta + \text{Im}C_1 \cos \theta] & -\hat{\varepsilon} & 0 \\ \hat{\varepsilon} [\text{Im}C_1 \sin \theta - (\text{Re}C_1 - C_2) \cos \theta] & 0 & -\hat{\varepsilon} \end{pmatrix}. \quad (\text{D19})$$

We are particularly interested in the case of evaluating the Jacobian at a fixed point. At a fixed point we have, using (D17) and (D18),

$$\begin{aligned} \text{Re}Q \cos \theta + \text{Im}Q \sin \theta &= -[(\text{Re}C_1 + C_2) \cos \theta - \text{Im}C_1 \sin \theta] \cos \theta \\ &\quad - [\text{Im}C_1 \cos \theta + (\text{Re}C_1 - C_2) \sin \theta] \sin \theta \\ &= -\text{Re}C_1 - C_2 \cos 2\theta, \end{aligned} \quad (\text{D20})$$

and thus,

$$J = \begin{pmatrix} \text{Re}C_1 + C_2 \cos 2\theta & -\sin \theta & \cos \theta \\ \hat{\varepsilon} [(\text{Re}C_1 + C_2) \sin \theta + \text{Im}C_1 \cos \theta] & -\hat{\varepsilon} & 0 \\ \hat{\varepsilon} [\text{Im}C_1 \sin \theta - (\text{Re}C_1 - C_2) \cos \theta] & 0 & -\hat{\varepsilon} \end{pmatrix}. \quad (\text{D21})$$

We can calculate the characteristic polynomial as

$$\begin{aligned} \chi(\lambda) &= [\text{Re}C_1 + C_2 \cos 2\theta - \lambda] (-\hat{\varepsilon} - \lambda)^2 - \hat{\varepsilon} [(\text{Re}C_1 + C_2) \sin \theta + \text{Im}C_1 \cos \theta] [-\sin \theta] [-\hat{\varepsilon} - \lambda] \\ &\quad - \hat{\varepsilon} [\text{Im}C_1 \sin \theta - (\text{Re}C_1 - C_2) \cos \theta] [-\hat{\varepsilon} - \lambda] [\cos \theta] \\ &= [\text{Re}C_1 + C_2 \cos 2\theta - \lambda] (\hat{\varepsilon} + \lambda)^2 + \hat{\varepsilon} [\hat{\varepsilon} + \lambda] [-(\text{Re}C_1 + C_2) \sin^2 \theta - \text{Im}C_1 \cos \theta \sin \theta + \text{Im}C_1 \sin \theta \cos \theta - (\text{Re}C_1 - C_2) \cos^2 \theta] \end{aligned}$$

$$\begin{aligned}
&= [\operatorname{Re}C_1 + C_2 \cos 2\theta - \lambda] (\hat{\varepsilon} + \lambda)^2 + \hat{\varepsilon} [\hat{\varepsilon} + \lambda] [-\operatorname{Re}C_1 + C_2 (\cos^2 \theta - \sin^2 \theta)] \\
&= (\hat{\varepsilon} + \lambda) \{ [\operatorname{Re}C_1 + C_2 \cos 2\theta - \lambda] (\hat{\varepsilon} + \lambda) + \hat{\varepsilon} [-\operatorname{Re}C_1 + C_2 \cos 2\theta] \} \\
&= (\hat{\varepsilon} + \lambda) \{ \operatorname{Re}C_1 \lambda + C_2 \cos 2\theta (\lambda + 2\hat{\varepsilon}) - \lambda^2 - \lambda \hat{\varepsilon} \} \\
&= -(\hat{\varepsilon} + \lambda) \{ \lambda^2 - \lambda [\operatorname{Re}C_1 + C_2 \cos 2\theta - \hat{\varepsilon}] - 2\hat{\varepsilon} C_2 \cos 2\theta \}.
\end{aligned} \tag{D22}$$

This means that one eigenvalue is always $\lambda_1 = -\hat{\varepsilon}$, which corresponds to a stable eigen-direction. In addition, we have two other eigenvalues, which we get as solutions of the quadratic equation

$$\lambda^2 - \lambda T + D = 0, \tag{D23}$$

$$T = \operatorname{Re}C_1 + C_2 \cos 2\theta - \hat{\varepsilon}, \tag{D24}$$

$$D = -2\hat{\varepsilon} C_2 \cos 2\theta, \tag{D25}$$

$$\lambda_{2/3} = \frac{T}{2} \pm \sqrt{\left(\frac{T}{2}\right)^2 - D}. \tag{D26}$$

We see that for $\theta_{0,1}$

$$\cos 2\theta_{0,1} \geq 0, \tag{D27}$$

$$D \leq 0. \tag{D28}$$

Therefore, $\theta_{0,1}$ is a saddle with two unstable directions and one stable direction. Similarly, $\theta_{0,3}$ is also a saddle. On the other hand, for $\theta_{0,2}$, we have

$$\cos 2\theta_{0,2} \leq 0, \tag{D29}$$

$$D \geq 0. \tag{D30}$$

The stability, therefore, depends on the sign of T . If $T < 0$, we have a stable node or focus with three stable directions; if $T > 0$, we have two unstable directions. At $T = 0$, we have a Hopf bifurcation. Let us express the condition for the Hopf in the original parameters of the system. At the fixed point, we have

$$C_2 \cos 2\theta_0 = \pm C_2 \sqrt{1 - \sin^2 2\theta_0} = \pm \sqrt{C_2^2 - (\operatorname{Im}C_1 - 1)^2} \tag{D31}$$

through (D4). Thus, the Hopf condition is given by

$$\operatorname{Re}C_1 - \hat{\varepsilon} = \mp \sqrt{C_2^2 - (\operatorname{Im}C_1 - 1)^2}, \tag{D32}$$

or more elegantly,

$$|C_1 - (\hat{\varepsilon} + i)| = C_2. \tag{D33}$$

4. Eigen-directions of the Jacobian matrix

The Jacobian matrix (D21) is remarkable in that at the fixed points, it only depends on the dynamical variable θ . We verify that

$$J \begin{pmatrix} 0 \\ \cos \theta \\ \sin \theta \end{pmatrix} = -\varepsilon \begin{pmatrix} 0 \\ \cos \theta \\ \sin \theta \end{pmatrix}, \tag{D34}$$

and therefore, the (slowly) stable eigen-direction with which we approach the fixed point is given by

$$v = \begin{pmatrix} 0 \\ \cos \theta \\ \sin \theta \end{pmatrix}. \tag{D35}$$

REFERENCES

- ¹K. Christensen, R. Donangelo, B. Koiller, and K. Sneppen, "Evolution of random networks," *Phys. Rev. Lett.* **81**, 2380 (1998).
- ²S. Bornholdt and T. Rohlf, "Topological evolution of dynamical networks: Global criticality from local dynamics," *Phys. Rev. Lett.* **84**, 6114 (2000).
- ³T. Gross and B. Blasius, "Adaptive coevolutionary networks: A review," *J. Roy. Soc. Interface* **5**, 259–271 (2008).
- ⁴R. Berner, T. Gross, C. Kuehn, J. Kurths, and S. Yanchuk, "Adaptive dynamical networks," *Phys. Rep.* **1031**, 1–59 (2023).
- ⁵J. Sawicki, R. Berner, S. A. Loos, M. Anvari, R. Bader, W. Barfuss, N. Botta, N. Brede, I. Franović, D. J. Gauthier *et al.*, "Perspectives on adaptive dynamical systems," *Chaos* **33**, 071501 (2023).
- ⁶H. Sayama, I. Pestov, J. Schmidt, B. J. Bush, C. Wong, J. Yamanoi, and T. Gross, "Modeling complex systems with adaptive networks," *Comput. Math. Appl.* **65**, 1645–1664 (2013).
- ⁷D. Hebb, *The Organization of Behavior. A Neuropsychological Theory* (John Wiley & Sons, 1949).
- ⁸S. Denève, A. Alemi, and R. Bourdoukan, "The brain as an efficient and robust adaptive learner," *Neuron* **94**, 969–977 (2017).
- ⁹A. Almaatouq, A. Noriega-Campero, A. Alotaibi, P. Krafft, M. Moussaid, and A. Pentland, "Adaptive social networks promote the wisdom of crowds," *Proc. Natl. Acad. Sci. U.S.A.* **117**, 11379–11386 (2020).
- ¹⁰P. Landi, H. O. Minoarivelo, Å. Brännström, C. Hui, and U. Dieckmann, "Complexity and stability of ecological networks: A review of the theory," *Popul. Ecol.* **60**, 319–345 (2018).
- ¹¹R. L. Raimundo, P. R. Guimarães, and D. M. Evans, "Adaptive networks for restoration ecology," *Trends Ecol. Evolut.* **33**, 664–675 (2018).
- ¹²Y. L. Maistrenko, B. Lysyansky, C. Hauptmann, O. Burylko, and P. A. Tass, "Multistability in the Kuramoto model with synaptic plasticity," *Phys. Rev. E* **75**, 066207 (2007).
- ¹³R. Gutiérrez, A. Amann, S. Assenza, J. Gómez-Gardenes, V. Latora, and S. Boccaletti, "Emerging meso- and macroscales from synchronization of adaptive networks," *Phys. Rev. Lett.* **107**, 234103 (2011).
- ¹⁴O. Burylko, Y. Kazanovich, and R. Borisyuk, "Winner-take-all in a phase oscillator system with adaptation," *Sci. Rep.* **8**, 416 (2018).
- ¹⁵A. Keane, A. Neff, K. Blaha, A. Amann, and P. Hövel, "Transitional cluster dynamics in a model for delay-coupled chemical oscillators," *Chaos* **33**, 063133 (2023).

- ¹⁶O. Burylko, A. Mielke, M. Wolfrum, and S. Yanchuk, "Coexistence of Hamiltonian-like and dissipative dynamics in rings of coupled phase oscillators with skew-symmetric coupling," *SIAM J. Appl. Dyn. Syst.* **17**, 2076–2105 (2018).
- ¹⁷F. Dörfler and F. Bullo, "Synchronization in complex networks of phase oscillators: A survey," *Automatica* **50**, 1539–1564 (2014).
- ¹⁸D. Kasatkina, S. Yanchuk, E. Schöll, and V. Nekorkin, "Self-organized emergence of multilayer structure and chimera states in dynamical networks with adaptive couplings," *Phys. Rev. E* **96**, 062211 (2017).
- ¹⁹R. Berner, E. Schöll, and S. Yanchuk, "Multiclusters in networks of adaptively coupled phase oscillators," *SIAM J. Appl. Dyn. Syst.* **18**, 2227–2266 (2019).
- ²⁰J. Fialkowski, S. Yanchuk, I. M. Sokolov, E. Schöll, G. A. Gottwald, and R. Berner, "Heterogeneous nucleation in finite-size adaptive dynamical networks," *Phys. Rev. Lett.* **130**, 067402 (2023).
- ²¹M. Cross, A. Zumdick, R. Lifshitz, and J. Rogers, "Synchronization by nonlinear frequency pulling," *Phys. Rev. Lett.* **93**, 224101 (2004).
- ²²Y. Maistrenko, O. Popovych, O. Burylko, and P. A. Tass, "Mechanism of desynchronization in the finite-dimensional Kuramoto model," *Phys. Rev. Lett.* **93**, 084102 (2004).
- ²³V. Pal, C. Tradonsky, R. Chriki, A. A. Friesem, and N. Davidson, "Observing dissipative topological defects with coupled lasers," *Phys. Rev. Lett.* **119**, 013902 (2017).
- ²⁴M. Yoshimoto, K. Yoshikawa, and Y. Mori, "Coupling among three chemical oscillators: Synchronization, phase death, and frustration," *Phys. Rev. E* **47**, 864 (1993).
- ²⁵I. Z. Kiss, Y. Zhai, and J. L. Hudson, "Emerging coherence in a population of chemical oscillators," *Science* **296**, 1676–1678 (2002).
- ²⁶M. Rohden, A. Sorge, M. Timme, and D. Witthaut, "Self-organized synchronization in decentralized power grids," *Phys. Rev. Lett.* **109**, 064101 (2012).
- ²⁷F. Molnar, T. Nishikawa, and A. E. Motter, "Network experiment demonstrates converse symmetry breaking," *Nat. Phys.* **16**, 351–356 (2020).
- ²⁸D. Witthaut, F. Hellmann, J. Kurths, S. Kettemann, H. Meyer-Ortmann, and M. Timme, "Collective nonlinear dynamics and self-organization in decentralized power grids," *Rev. Mod. Phys.* **94**, 015005 (2022).
- ²⁹L. Huo and X. Chen, "Higher-order motif-based time series classification for forced oscillation source location in power grids," *Nonlinear Dyn.* **111**, 20127–20138 (2023).
- ³⁰A. Pluchino, V. Latora, and A. Rapisarda, "Changing opinions in a changing world: A new perspective in sociophysics," *Int. J. Mod. Phys. C* **16**, 515–531 (2005).
- ³¹K. Vasudevan, M. Cavers, and A. Ware, "Earthquake sequencing: Chimera states with Kuramoto model dynamics on directed graphs," *Nonlinear Process Geophys.* **22**, 499–512 (2015).
- ³²S. H. Strogatz, "From Kuramoto to Crawford: Exploring the onset of synchronization in populations of coupled oscillators," *Phys. D* **143**, 1–20 (2000).
- ³³J. A. Acebrón, L. L. Bonilla, C. J. P. Pérez Vicente, F. Ritort, and R. Spigler, "The Kuramoto model: A simple paradigm for synchronization phenomena," *Rev. Mod. Phys.* **77**, 137 (2005).
- ³⁴F. A. Rodrigues, T. K. D. Peron, P. Ji, and J. Kurths, "The Kuramoto model in complex networks," *Phys. Rep.* **610**, 1–98 (2016).
- ³⁵J. Wu and X. Li, "Collective synchronization of Kuramoto-oscillator networks," *IEEE Circuits Syst. Mag.* **20**, 46–67 (2020).
- ³⁶A. E. Motter, C. Zhou, and J. Kurths, "Network synchronization, diffusion, and the paradox of heterogeneity," *Phys. Rev. E* **71**, 016116 (2005).
- ³⁷A. Arenas, A. Díaz-Guilera, J. Kurths, Y. Moreno, and C. Zhou, "Synchronization in complex networks," *Phys. Rep.* **469**, 93–153 (2008).
- ³⁸S. Boccaletti, A. N. Pisarchik, C. I. Del Genio, and A. Amann, *Synchronization: From Coupled Systems to Complex Networks* (Cambridge University Press, 2018).
- ³⁹S. H. Strogatz and I. Stewart, "Coupled oscillators and biological synchronization," *Sci. Am.* **269**, 102–109 (1993).
- ⁴⁰B. Blasius, A. Huppert, and L. Stone, "Complex dynamics and phase synchronization in spatially extended ecological systems," *Nature* **399**, 354–359 (1999).
- ⁴¹D. J. Watts and S. H. Strogatz, "Collective dynamics of 'small-world' networks," *Nature* **393**, 440–442 (1998).
- ⁴²D. M. Abrams, L. M. Pecora, and A. E. Motter, "Introduction to focus issue: Patterns of network synchronization," *Chaos* **26**, 094601 (2016).
- ⁴³M. Thiele, R. Berner, P. A. Tass, E. Schöll, and S. Yanchuk, "Asymmetric adaptivity induces recurrent synchronization in complex networks," *Chaos* **33**, 023123 (2023).
- ⁴⁴M. Rolim Sales, S. Yanchuk, and J. Kurths, "Recurrent chaotic clustering and slow chaos in adaptive networks," *Chaos* **34**, 063144 (2024).
- ⁴⁵V. N. Belykh, G. V. Osipov, V. S. Petrov, J. A. Suykens, and J. Vandewalle, "Cluster synchronization in oscillatory networks," *Chaos* **18**, 037106 (2008).
- ⁴⁶X. W. Liu and T. P. Chen, "Finite-time and fixed-time cluster synchronization with or without pinning control," *IEEE Trans. Cybernetics* **48**, 240–252 (2016).
- ⁴⁷F. Della Rossa, L. Pecora, K. Blaha, A. Shirin, I. Klickstein, and F. Sorrentino, "Symmetries and cluster synchronization in multilayer networks," *Nat. Commun.* **11**, 3179 (2020).
- ⁴⁸J. Rinzel, "Bursting oscillations in an excitable membrane model," in *Ordinary and Partial Differential Equations: Proceedings of the Eighth Conference, Dundee, June 25–29, 1984* (Springer, 2006), pp. 304–316.
- ⁴⁹E. M. Izhikevich, "Neural excitability, spiking and bursting," *Int. J. Bifur. Chaos* **10**, 1171–1266 (2000).
- ⁵⁰X. J. Han and Q. S. Bi, "Bursting oscillations in Duffing's equation with slowly changing external forcing," *Commun. Nonlinear Sci. Numer. Simul.* **16**, 4146–4152 (2011).
- ⁵¹C. Batista, S. R. Lopes, R. L. Viana, and A. M. Batista, "Delayed feedback control of bursting synchronization in a scale-free neuronal network," *Neural Netw.* **23**, 114–124 (2010).
- ⁵²D. Fan and Q. Wang, "Synchronization and bursting transition of the coupled Hindmarsh-Rose systems with asymmetrical time-delays," *Sci. China Technol. Sci.* **60**, 1019–1031 (2017).
- ⁵³R. Li, B. L. Xu, D. B. Chen, J. F. Zhou, and W. J. Yuan, "Transitions to synchronization induced by synaptic increasing in coupled tonic neurons with electrical synapses," *Chaos, Solitons Fractals* **176**, 114104 (2023).
- ⁵⁴P. Seliger, S. C. Young, and L. S. Tsimring, "Plasticity and learning in a network of coupled phase oscillators," *Phys. Rev. E* **65**, 041906 (2002).
- ⁵⁵T. Aoki and T. Aoyagi, "Co-evolution of phases and connection strengths in a network of phase oscillators," *Phys. Rev. Lett.* **102**, 034101 (2009).
- ⁵⁶N. Fenichel, "Geometric singular perturbation theory for ordinary differential equations," *J. Diff. Equ.* **31**, 53–98 (1979).
- ⁵⁷G. Boffetta, A. Crisanti, F. Paparella, A. Provenzale, and A. Vulpiani, "Slow and fast dynamics in coupled systems: A time series analysis view," *Phys. D* **116**, 301–312 (1998).
- ⁵⁸C. Kuehn *et al.*, *Multiple Time Scale Dynamics* (Springer, 2015), Vol. 191.
- ⁵⁹T. Witelski and M. Bowen, "Fast/slow dynamical systems," in *Methods of Mathematical Modelling: Continuous Systems and Differential Equations* (Springer International Publishing, Cham, 2015), pp. 201–213.
- ⁶⁰J.-M. Ginoux, "Slow invariant manifolds of slow-fast dynamical systems," *Int. J. Bifurc. Chaos* **31**, 2150112 (2021).
- ⁶¹Y. Kuramoto, *Chemical Oscillations, Waves, and Turbulence* (Springer, 1984).
- ⁶²M. A. Armstrong, *Groups and Symmetry* (Springer Verlag, 1988).